The Behavior of a Power-Law Fluid Flowing Through a Sudden Expansion

Part II. Experimental Verification

Experimental data are presented to verify the numerical model discussed in Part I. The experimental techniques employed for recovering flow patterns and for point velocity measurement are described and justified. The measured reattachment lengths, the recorded flow patterns, and the developing axial velocity field all show excellent agreement with the model predictions.

A. L. HALMOS
and
D. V. BOGER

Department of Chemical Engineering,
Monash University
Clayton, Victoria, Australia

EXPERIMENTAL TECHNIQUE AND APPARATUS

The characteristics of the secondary cell and the details of the point velocity field were experimentally investigated for flow of inelastic power law fluids through an abrupt 1 to 2 expansion. The experimental results were then compared to numerical predictions obtained from the models already discussed.

The flow system used, show in Figure 1, consisted of an 18 m^3 storage tank fitted with an air stirrer, an 11 kW variable speed monopump, a surge tank, a 0.22 m^3 drum on a 250 Kg platform scale, and a transparent 3.3m long test section, housed in a long rectangular box framework. The test fluid was pumped from the storage tank through the test section, and either directly back into the storage tank, or into a drum on the platform scale before being returned by gravity to the storage tank.

Copper-constantan thermocouples, located before and after the test section, were employed to measure the temperature of the circulating test fluids. Data were discarded when the temperature varied by more than 1C° over the length of the section.

A Fisher-Porter magnetic flow meter, calibrated by the accumulation of mass in the drum on the platform scale, was used for flow rate measurement.

The test section, shown schematically in Figure 2, was designed so that flow visualization studies and point velocity measurement could be made in the entire 1 to 2 expansion. A 25.4-mm I.D. precision bore glass tube was fitted into a perspex piece whose I.D. was 125 μm greater than the O.D. of the glass tube. The optically clear join between the glass and perspex was formed with Cellulose Caprate Gum. Heating was employed to expand the perspex piece which was slipped over the glass tube while the gum was applied. Two 1.5m lengths of 50.8-mm I.D. precision bore glass tube were then forced over O-rings which were placed in grooves on the perspex piece. A high viscosity silicone oil was used as lubricant and clearance filler. The clearance between the perspex and the I.D. of the glass tube was 50 μm. A central ring which fitted between the two larger glass tubes was left on the perspex. The smaller tube was held concentric with the larger tube by the perspex piece (which also formed the abrupt expansion) and by a cylindrical disk at the extreme upstream end of the test section.

Streak photography, using a continuous light source and previously reported techniques (Rama Murthy and Boger, 1971), was used for flow visualization studies and for determining the size of the secondary cell. Streak photography was not used for point velocity measurement because of the ill-defined ends of the streaks produced as a result of the opening and closing of the camera shutter and because of overheating of the optical system which occurred with prolonged use of the high intensity light source. Instead two flash tubes were used as light sources and were triggered at an electronically preset time interval. The shutter of the Exacta 35-mm camera was opened for a time period within which the two flashes were triggered. Because of reflection from the tracer particles in the test fluid, the flashes produced two comet-like dots on the photograph with clearly defined heads. A flash photograph of one half of the 1 to 2 expansion illustrating the dots and the secondary flow is shown in Figure 3. With knowledge of the time interval between flashes, the magnification, and the system dimensions, the point velocities were determined with the use of an X-Y data reader. Further details on the optical system, the electronic circuit, and its calibration are available (Halmos, 1973).

Methocel 90HG (Dow Chemical) was used as a test fluid because optically clear solutions with a wide range of non-Newtonian behavior can be produced by varying the concentration in water. In addition, Methocel is not prone to shear

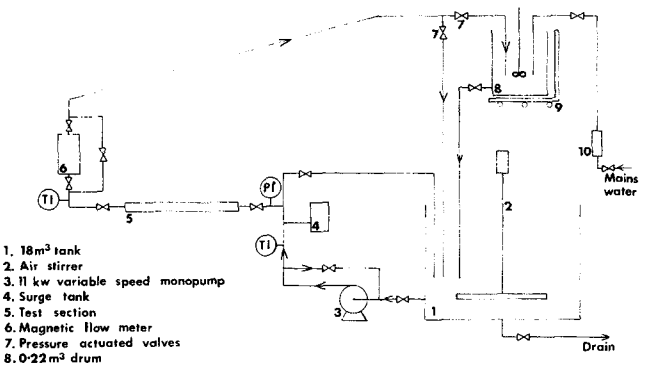

Fig. 1. Schematic diagram of flow system.

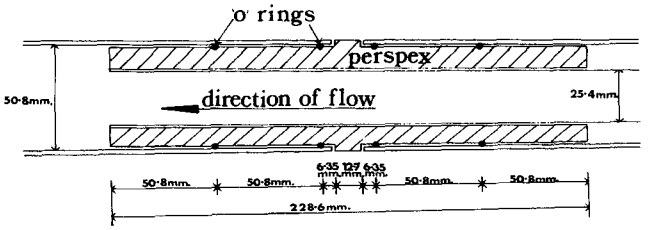

Fig. 2. Detail of test section at plane of expansion.

A. L. Halmos is with the Department of Chemical Engineering and Chemical Technology, Imperial College, London, SW7 2AZ, England.

degradation in the flow system (Rama Murthy and Boger, 1971) Mearlin A. (Mearl Corp., N.Y.) was used as the tracer particle.

The shear stress as a function of shear rate was measured for a sample of test fluid taken before and after each run on the flow system. Agreement between the two sets of data indicated the absence of shear degradation. An R16 Weissenberg Rheogoniometer in cone and plate configuration was used for these measurements. Errors associated with evaporation of the test sample were eliminated (Boger and Rama Murthy, 1969). A check was also made to ensure that the Methocel solution did not exhibit appreciable elasticity. Solutions were chosen so that no measurable first normal stress difference (less than 100 dyne/cm^2) was observed at the maximum shear rates encountered in the test section. The flow behavior index n and the consistency factor k were determined from the slope and the intercept of the log-log plot of shear stress versus shear rate. Fluid characterizations were carried out over the maximum shear rate range observed in the test section and over the range of temperatures (15° to 25°C) encountered in the flow system. n was found to vary by less than 3% over this temperature range while k was corrected to the temperature in the flow system by interpolation on an Arrhenius plot of log k versus $1/T$. The modified Reynolds number for each experimental run was calculated from

$$Re_{\text{mod}} = \frac{\rho D^n W^{2-n}}{k} \qquad (1)$$

where W = average velocity in the upstream tube and D = upstream tube diameter.

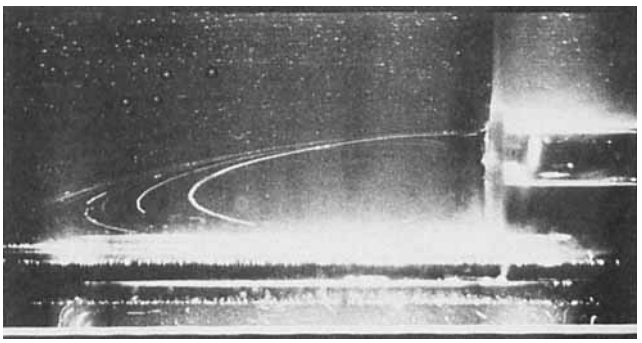

Fig. 3. Example of flash photograph showing secondary cell.

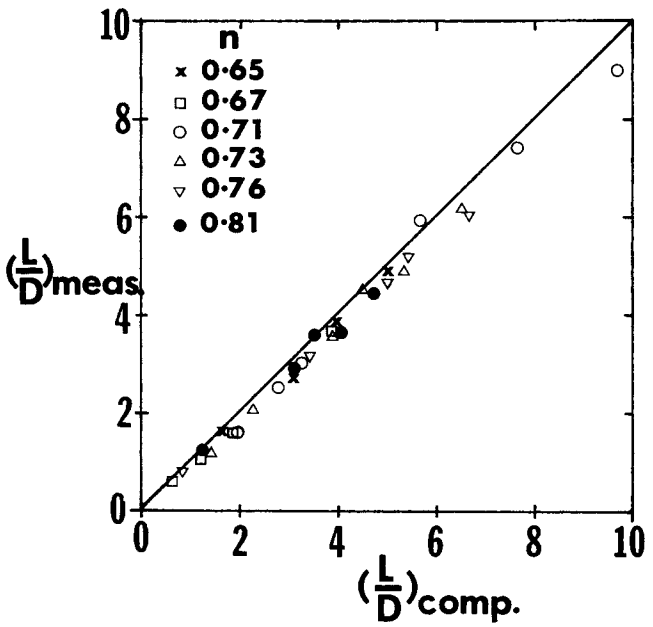

Fig. 4. Comparison of experimentally measured and numerically predicted reattachment lengths.

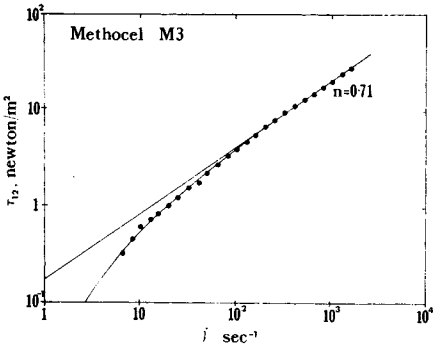

Fig. 5. Example of a flow curve for a Methocel solution.

RESULTS AND DISCUSSION

The reattachment length and developing velocity profiles were measured for six different inelastic Methocel solutions for $0.65 \leq n \leq 0.81$ and for $6.7 \leq Re_{\text{mod}} \leq 158.8$. Each set of experimental results was then reproduced at the same n and Re_{mod} on the computer by using either the RT-RT model or the ST-RT model (See Part I). The experimental and numerical results were then compared.

Reattachment Lengths and Flow Patterns

Figure 4 shows a comparison of the experimentally measured to the numerically predicted reattachment lengths. The experimental L/D varied from 0.53 to 9.00. The experimental results are consistently lower than the numerical results by an average of 7%. This difference arises because of the inadequateness of the power-law model as the shear rate approaches zero. Figure 5 shows a representative log-log plot of the shear stress versus the shear rate (flow curve) for one of the Methocel solutions. Note that n increases as the shear rate decreases with Newtonian behavior ($n = 1$) being approached in the limit. In the numerical model n was evaluated from the slope of the flow curve in the shear rate range coinciding with the wall shear rate for fully developed flow in the upstream and down stream tubes. For Methocel M3, the conditions in the contraction corresponded to $n = 0.71$ as shown in Figure 5. However, the shear rate encountered near the reattachment point approaches zero and the solution approaches Newtonian behavior. Therefore using $n = 0.71$ in the numerical model does not accurately represent the fluid near the reattachment point where a higher value prevails. Since the reattachment length decreases with increasing n (See Part I), it is not surprising that the observed reattachment lengths are slightly lower than the predicted ones. The flow behavior index could be varied with shear rate in the numerical model, but the significant increase in computation time that results is not warranted because of the small errors involved.

Figures 6 and 7 show the experimentally observed flow patterns with the numerical results for the predicted stream function superimposed on the upper half of the photograph. A RT-RT model was used for the experimental conditions of $n = 0.76$ and $Re_{\text{mod}} = 11.2$ as shown in Figure 6 and a ST-RT model was used for $n = 0.73$ and $Re_{\text{mod}} = 21.6$ in Figure 7. Good agreement is obtained between the experimentally observed and the numerically predicted flow patterns.

Velocity Field

The next step in verifying the numerical models was a comparison of the measured point velocities to those produced using the models. In order to establish the

measurement techniques and to evaluate the accuracy of the data obtained, fully developed axial velocity profiles were measured both upstream and downstream of the plane of expansion for all fluids tested. Figure 8 shows a comparison of the measured fully developed profiles in the upstream and downstream tube to the predicted profiles for $21.6 \leq Re_{mod} \leq 121.0$ and $n = 0.73$. The average velocity determined from integrating the measured velocity profile always agreed to within 3% of the measured average velocity. The excellent agreement of the measured velocity profiles with the predicted velocity profiles and of the integrated velocity profile with the measured average velocity serves to justify and establish the level of errors involved in the point velocity data to be presented.

The development of the center line velocity from fully developed flow in the 25.4-mm I.D. tube to fully developed flow in the 50.8-mm I.D. tube was measured for the six test fluids. A comparison of the measured to the predicted center line velocity for one of the fluids is shown in Figure 9 for $n = 0.76$ and $11.2 \leq Re_{mod} \leq 123.8$. Similar excellent agreement between the measured and predicted center line velocities was obtained for $0.65 \leq n \leq 0.81$ and for $6.7 \leq Re_{mod} \leq 158.8$. Note in Figure 9 the slight predevelopment of the center line velocity for $Re_{mod} = 11.2$ and its prediction by the RT-RT model. Since the measurement of point velocities is dependent on the chance that a particle passes through the right plane at the right time, the number of velocity measurements taken exactly at the center line was small. The center line velocity measurements were therefore taken within a band of $\pm 0.05\ D$. The error, estimated from the theoretically predicted profiles, produced by this band was 1% for the worst case.

Good agreement was also obtained between the measured developing axial velocity profiles and the numerical prediction. Figures 10 and 11 show a typical comparison for $n = 0.73$ and $Re_{mod} = 121.0$. The closed points represent point velocities measured in the lower half of the tube, and the open points are for the upper half. Note the agreement of the upper and lower half velocity measurements, thus illustrating the symmetry of the flow field.

Since the length of the slit of light photographed was 50.8 mm, point velocity measurements were taken over

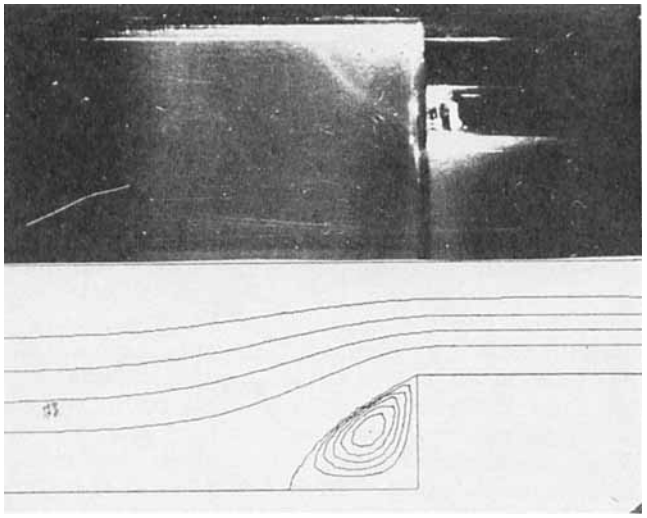

Fig. 6. Comparison of observed streamlines to the numerical prediction for $n = 0.76$ and $Re_{mod} = 11.2$.

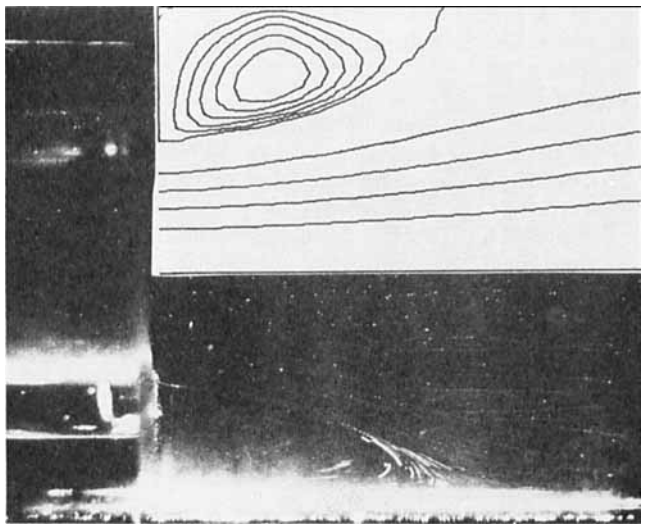

Fig. 7. Comparison of the observed streamlines to the numerical prediction for $n = 0.73$ and $Re_{mod} = 21.6$.

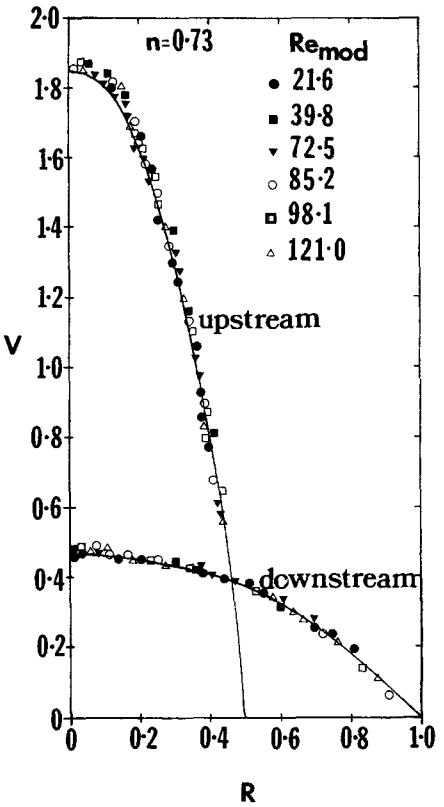

Fig. 8. Fully developed velocity profiles upstream and downstream of the expansion for $n = 0.73$ and $21.6 \leq Re_{mod} \leq 121.0$.

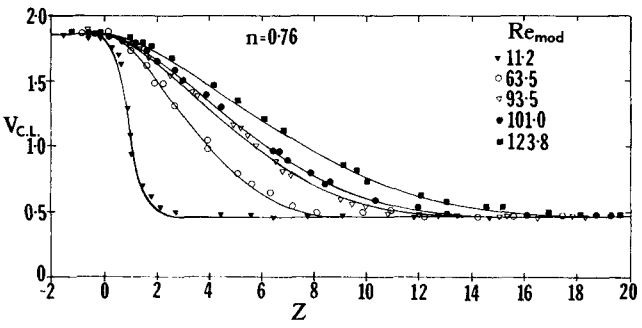

Fig. 9. Comparison of the observed center line velocity development to the numerical predictions.

a finite length of the tube. Therefore, to be able to compare a measured and predicted velocity profile at any particular axial plane, an enormous number of photographs would have to be taken to obtain sufficient point velocities, or a finite length of tube would have to be considered as a plane and the experimental results compared to a band of predicted velocity profiles at the two ends of the finite experimental length. The latter method was chosen. The two extremes of the numerical prediction were drawn and the experimental velocities measured in that region were plotted using the same dimensionless variables, that is, with respect to the smaller tube diameter and the average velocity in the smaller tube. The choice of band width was dictated by numerical and experimental errors. Numerically predicted velocity profiles were chosen such that the two extremes of the numerical prediction were ± 5% about the mean value.

Velocities were not measured inside the secondary cell because of the highly curved path of the tracer particles which existed in this region, making the recognition of pairs of points necessary for velocity measurements impractical. The radial velocity component outside the secondary cell was also not measured because its magnitude was about 1 to 5% of the axial velocity component and hence too small to measure accurately.

ACKNOWLEDGMENT

The authors are grateful to the Australian Research Grants Commission for their financial support and to B. Blake for her help in preparation of the manuscript.

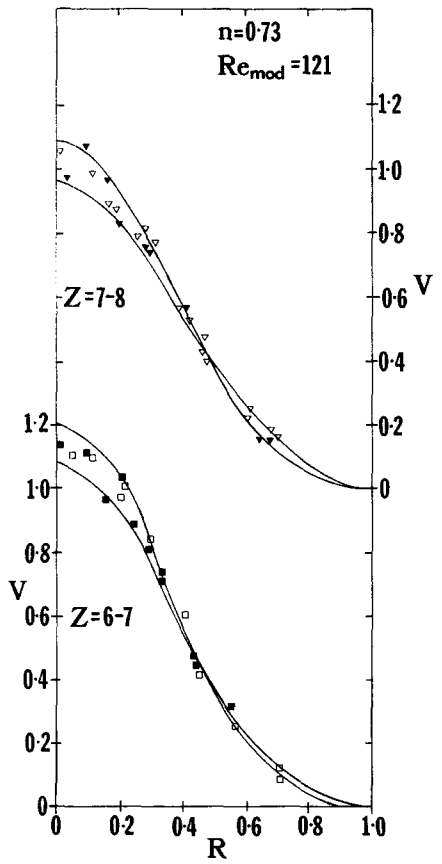

Fig. 10. Comparison of the measured developing axial velocity profiles to the numerical prediction in a region close to the reattachment point for n = 0.73 and Re_{mod} = 121.0.

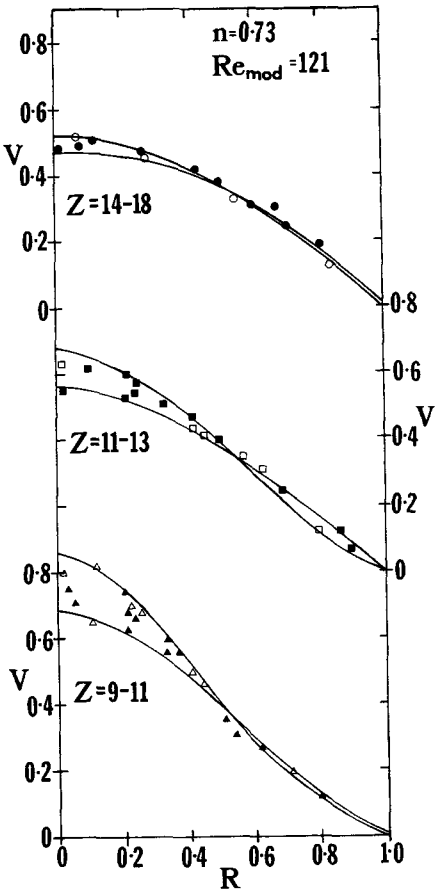

Fig. 11. Comparison of the measured developing velocity profiles to the numerical prediction in a downstream region removed from the reattachment point for n = 0.73 and Re_{mod} = 121.0.

NOTATION

D = diameter of upstream tube
k = consistency index in power law
L = reattachment length
n = flow behavior index in power law
r = radial distance
R = dimensionless radial coordinate, r/D
v_z = axial velocity
V = dimensionless axial velocity, v_z/W
V_{CL} = dimensionless center line velocity
W = average velocity in upstream tube
z = axial distance
Z = dimensionless axial coordinate, z/D

Greek Letters

$\dot{\gamma}$ = shear rate
ρ = fluid density
τ = shear stress

LITERATURE CITED

Boger, D. V., and A. V. Rama Murthy, "Normal Stress Measurement and Evaporation Effects on the Weissenberg Rheogoniometer," *Trans. Soc. Rheol.*, 13, 405 (1969).

Halmos, A. L. "The Flow of Viscous and Viscoelastic Fluids Through an Abrupt Expansion," Ph.D. thesis, Monash Univ., Melbourne (1973).

Rama Murthy, A. V., and D. V. Boger, "Developing Velocity Profiles on the Downstream Side of a Contraction for Inelastic Polymer Solutions," *Trans. Soc. Rheol.*, 15, 709 (1971).

Manuscript received December 3, 1974; revision received January 28 and accepted January 29, 1975.